Phase Separation Dynamics and Reaction Kinetics of Ternary Mixture Coupled with Interfacial Chemical Reaction

Chaohui Tong, Hongdong Zhang, and Yuliang Yang*

Department of Macromolecular Science, Key Lab of Molecular Engineering of Polymers, SMEC, Fudan University, Shanghai 200433, China

Received: March 11, 2002; In Final Form: June 6, 2002

In this paper, computer simulation results of phase separation dynamics of ternary mixture (A, B, and C) coupled with an interfacial chemical reaction A + B═C in two-dimension are presented. The effect of reduction of interfacial free energy due to the presence of species C along the interface is taken into consideration in our study. In the case of fixed domain size, it is shown in simulations that for both reversible and irreversible reactions the generation of species C is not affected by the reaction rate constants, and it is a diffusion-controlled process. Also, the simulation reveals that for reversible chemical reaction in the case of fixed domain size, the equilibrium of concentrations is established. In the cases of coupling between domain growth and reversible reaction kinetics, it is shown in simulations that the domain growth eventually freezes regardless of the magnitude of the reaction rate constants. The higher the reaction rate constants are, the slower the evolution to reach the reach steady state is, the larger the steady state domain size is, and the smaller the average concentration of species C is.

I. Introduction

The self-assemblies of amphiphilic systems are interesting and important from both theoretical and industrial points of view and have attracted much attention.[1,2] The two most important amphiphilic systems are oil/water with surfactants and type A and B immiscible polymer blends with type A−B block copolymers. The amphiphilic molecules/macromolecules segregating on the interface between the two immiscible phases can lower the surface tension and enhance interfacial adhesion; therefore, they serve effectively as phase compatibilizers. Most polymer pairs are immiscible and phase separate into macroscopic domains, resulting in poor mechanical properties of the blends. Therefore, blending of existing homopolymers with the aid of block copolymers is attractive as one means to create new materials at relatively low cost. One more promising way to make polymer blends is the process of reactive blending.[3−6] An important feature of reactive blending is the in situ production of block copolymers in the interfacial regions, rendering the separate expensive copolymer synthesis unnecessary. Also, this process overcomes the problem of slow diffusion of the block copolymer to the interface in homopolymer blending with block copolymer. The copolymers generated on the interface would be linear diblock copolymers in the case where the reactive groups are at the chain ends of the two homopolymers and can increase the interfacial strength and are believed to promote mixing in an additional way, which slows down the coalescence rates of droplets of one phase dispersed in another phase through steric repulsion.

In our previous papers concerning the coupling of phase separation and chemical reaction,[7,8] we studied the chemical reaction kinetics and phase separation dynamics of a ternary mixture A, B, and C coupled with reversible reaction of type A + B ⇌ C, where we assumed that A, B, and C possess the normal Flory−Huggins-type interaction. In the case that species C is relatively compatible with both A and B, whereas A and B are quite incompatible with each other, simulation reveals that the phase separation between A and B pushes species C to the interface, where species C decomposes exponentially with evolution time and the exponent is proportional to the magnitude of reaction rate constant. Eventually, the initial ternary mixture system consisting of A, B, and C transforms into an ordinary binary mixture system composed of A and B without the involvement of chemical reaction. However, for the amphiphilc system, the effect of lowering of interfacial tension of the amphiphilic molecules/macromolecules is very important and needs to be considered. Computer simulations of the oil/water/surfactant system reveal that phase separation between oil and water slows down and eventually freezes due to the effect of reduction of the interfacial tension of the surfactants.[9−12]

The purpose of this paper is to study the reaction kinetics and phase separation dynamics in ternary mixture A, B, and C coupled with reaction of A + B ⇌ C with the inclusion of the effect of reduction of interfacial tension of species C. Extensive simulation is performed up to 3 million time steps to clearly identify the domain growth dynamics. The paper is organized as follows. Section II derives the model equations starting from the equation of continuity and describes simulation schemes in two dimensions. Section III presents the simulation results and discussions. Finally, in section IV, we draw major conclusions of the present study.

II. Model Equations and Simulation Schemes

We are considering the phase separation of a ternary mixture composed of species A, B and C, which simultaneously undertake a reversible chemical reaction

$$A + B \underset{\Gamma_{-1}}{\overset{\Gamma_1}{\rightleftharpoons}} C$$

* To whom all correspondence should be addressed. E-mail: ylyang@srcap.stc.sh.cn.

10.1021/jp020668v CCC: $22.00
Published on Web 07/19/2002

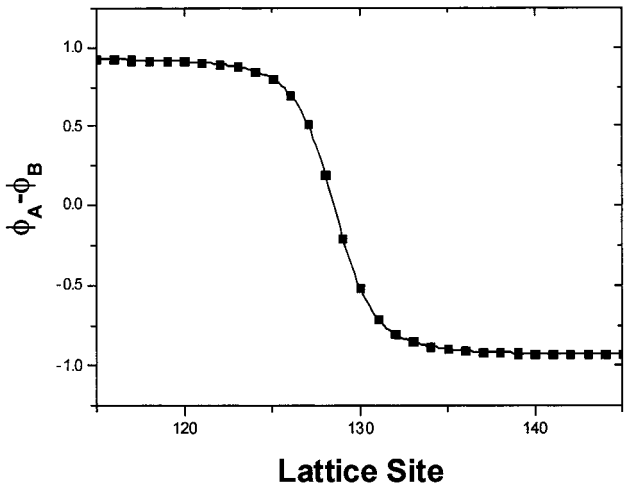

Figure 1. Profile of the order parameter in the direction perpendicular to the interface at time step 1k.

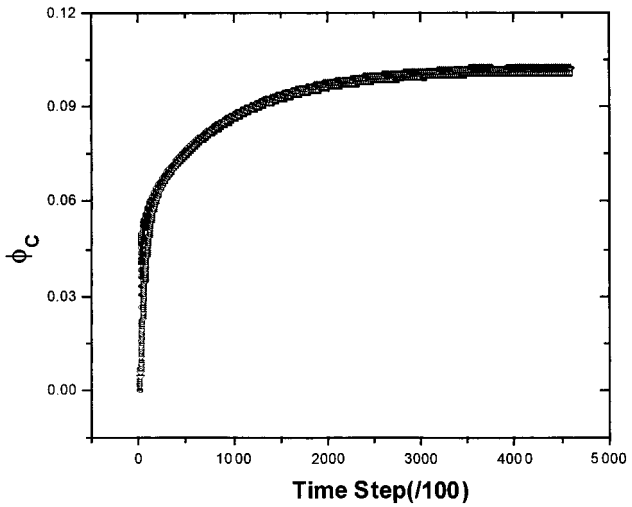

Figure 2. Time evolution profile of the average concentration of species C at different reaction rate constants (0.1, 0.01, 0.001, 0.0001, and 0.00001).

where $\Gamma_{\pm 1}$ are the forward and backward reaction rate constants. The reaction is confined to the interface between A and B, where species C acts as a compatibilizer for both A and B. For simplicity, we assume A and B have the same molecular weight and size, whereas C has twice as much molecular weight and size as A or B. The molar concentrations and the volume fraction of A, B, and C are donated as C_A, C_B, and C_C, and ϕ_A, ϕ_B, and ϕ_C, respectively. Obviously, volume fractions satisfy the following equation:

$$\phi_A + \phi_B + \phi_C = 1 \tag{1}$$

Mass transfer equations in terms of molar concentrations are

$$\frac{\partial}{\partial t}C_A + \nabla\cdot(C_A\mathbf{V}_A) = \Gamma_{-1}C_C - \Gamma_1 C_A C_B \tag{2}$$

$$\frac{\partial}{\partial t}C_B + \nabla\cdot(C_B\mathbf{V}_B) = \Gamma_{-1}C_C - \Gamma_1 C_A C_B \tag{3}$$

$$\frac{\partial}{\partial t}C_C + \nabla\cdot(C_C\mathbf{V}_C) = \Gamma_1 C_A C_B - \Gamma_{-1}C_C \tag{4}$$

where $\mathbf{v}_\alpha$ (α = A, B, and C) is the velocity of the component A, B, or C, respectively.

Summation of eqs 2−4 affords

$$\frac{\partial}{\partial t}C + \nabla\cdot(C\mathbf{V}) = \Gamma_{-1}C_C - \Gamma_1 C_A C_B \tag{5}$$

where $C = C_A + C_B + C_C$, and $\mathbf{V} = \{(C_A\mathbf{V}_A + C_B\mathbf{V}_B + C_C\mathbf{V}_C)\}/\{C\}$.

With the assumption about the molecular weights and sizes of A, B, and C, the volume fractions are related to the molar concentrations via:

$$\phi_A = \frac{C_A}{C_A + C_B + 2C_C} \tag{6}$$

$$\phi_B = \frac{C_B}{C_A + C_B + 2C_C} \tag{7}$$

$$\phi_C = \frac{2C_C}{C_A + C_B + 2C_C} \tag{8}$$

We now define $C^* = C_A + C_B + 2C_C$, which is a constant under incompressible condition. Then eqs 2−4 can be transformed to following mass transfer equations in terms of volume fractions:

$$\frac{\partial}{\partial t}\phi_A + \nabla\cdot(\phi_A\mathbf{V}_A) = (\{\Gamma_{-1}\}/\{2\})\phi_C - (C*\Gamma_1)\phi_A\phi_B \tag{9}$$

$$\frac{\partial}{\partial t}\phi_B + \nabla\cdot(\phi_B\mathbf{V}_B) = (\{\Gamma_{-1}\}/\{2\})\phi_C - (C*\Gamma_1)\phi_A\phi_B \tag{10}$$

$$\frac{\partial}{\partial t}\phi_C + \nabla\cdot(\phi_C\mathbf{V}_C) = (2C^*\Gamma_1)\phi_A\phi_B - \Gamma_{-1}\phi_C \tag{11}$$

Summation of eqs 9−11 gives

$$\nabla\cdot\mathbf{V}^* = 0 \tag{12}$$

where $\mathbf{V}^* = \phi_A\mathbf{V}_A + \phi_B\mathbf{V}_B + \phi_C\mathbf{V}_C$. Obviously, $\mathbf{V}^* \neq \mathbf{V}$.

Now, without loss of generality, we define the following two independent order parameters:

$$\psi = \phi_A - \phi_B \tag{13}$$

$$\varphi = \phi_C \tag{14}$$

Subtraction of eq 9 by eq 10 gives

$$\frac{\partial}{\partial t}\psi + \nabla\cdot(\psi\mathbf{V}_\psi) = 0 \tag{15}$$

with

$$\mathbf{V}_\psi = \frac{\phi_A\mathbf{V}_A - \phi_B\mathbf{V}_B}{\psi} \tag{16}$$

Now, we employ the Rayleigh's variational method introduced by Doi[13] and used in the study of microemulsion by Ohta.[14] The variational functional in the present system is given by

$$K = \frac{W}{2} + \dot{F}\{\psi,\varphi\} - \int \mathrm{d}r\, P(r,t)\nabla\cdot\mathbf{V}^* \tag{17}$$

where P is the Lagrange multiplier to take into account of the constraint eq 12. W is the Rayleigh's dissipation function given by

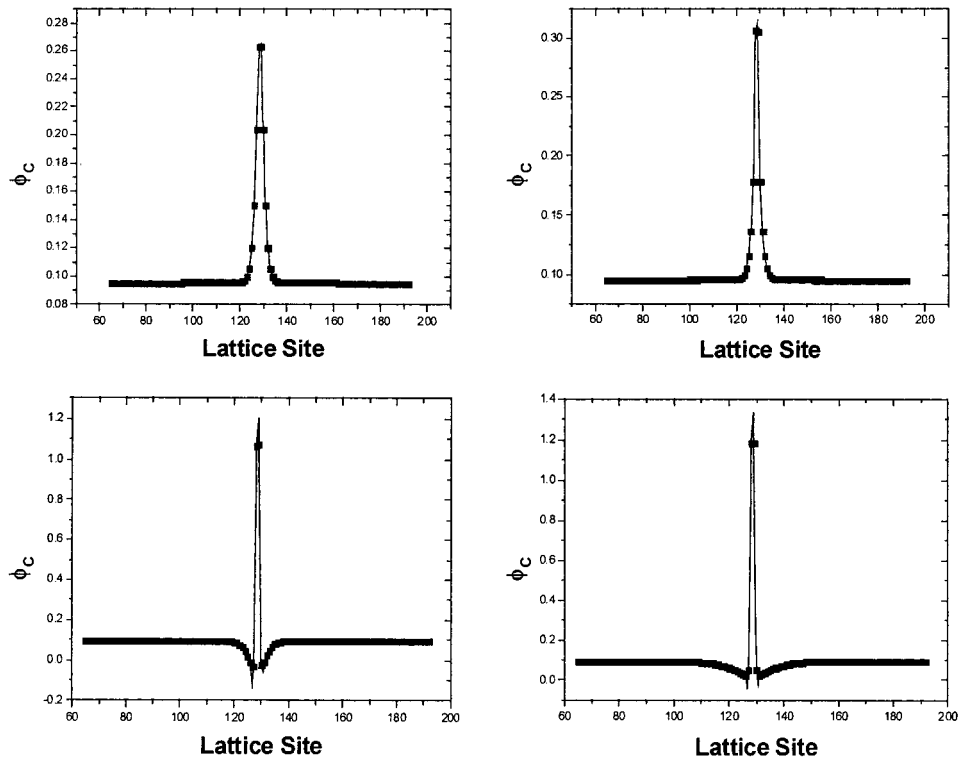

Figure 3. Steady-state concentration profile of species C along the direction perpendicular to the interface at different reaction rate constants. Top row: 0.1 for left, 0.01 for right. Bottom row: 0.001 for left, 0.0001 for right.

$$W = \int \mathrm{d}r\{\xi_1(\mathbf{V}_A - \mathbf{V}_B)^2 + \xi_2(\mathbf{V}_B - \mathbf{V}_C)^2 + \xi_3(\mathbf{V}_A - \mathbf{V}_C)^2 + \eta(\nabla\mathbf{V}^*:\nabla\mathbf{V}^*)\} \quad (18)$$

where ξ_i are the friction constants for the relative motion of pair of components. The last term stands for the viscous dissipation with η the viscosity.

The second term is eq 17 is the time derivative of the free energy functional and is explicitly given in terms of independent variables ψ,φ:

$$\dot{F} = \int \mathrm{d}r\left[\frac{\delta F}{\delta\psi}\frac{\partial\psi}{\partial t} + \frac{\delta F}{\delta\varphi}\frac{\partial\varphi}{\partial t}\right] = \int \mathrm{d}r\left[\psi\mathbf{V}_\psi\cdot\nabla\frac{\delta F}{\delta\psi}\right] + \frac{\delta F}{\delta\varphi}\left[2C^*\Gamma_1\frac{(1+\psi-\varphi)}{2}\frac{(1-\psi-\varphi)}{2} - \Gamma_{-1}\varphi - \nabla\cdot(\varphi\mathbf{V}_C)\right] \quad (19)$$

where we have used the continuity equations (15) and (11) for ψ,φ as well as the relations:

$$\phi_A = \frac{1+\psi-\varphi}{2}$$
$$\phi_B = \frac{1-\psi-\varphi}{2}$$
$$\phi_C = \varphi \quad (20)$$

Now we take the variation of K with respect to $\mathbf{V}^*$, $\mathbf{V}_\psi$, and $\mathbf{V}_C$:

$$\frac{\delta K}{\delta\mathbf{V}^*} = 0 \quad (21)$$

$$\frac{\delta K}{\delta\mathbf{V}_\psi} = 0 \quad (22)$$

$$\frac{\delta K}{\delta\mathbf{V}_C} = 0 \quad (23)$$

Summation of above three equations gives

$$\eta\nabla^2\mathbf{V}^* - \nabla p - \psi\nabla\frac{\delta F}{\delta\psi} - \varphi\nabla\frac{\delta F}{\delta\varphi} = 0 \quad (24)$$

In the above equation, inertial contribution is neglected. If we include inertial term, we arrive at

$$\frac{\partial\mathbf{V}^*}{\partial t} + (\mathbf{V}^*\cdot\nabla)\mathbf{V}^* = \eta\nabla^2\mathbf{V}^* - \nabla p - \psi\nabla\frac{\delta F}{\delta\psi} - \varphi\nabla\frac{\delta F}{\delta\varphi} \quad (25)$$

From (22) and (23), we obtain

$$\mathbf{V}_\psi - \mathbf{V}^* = M_{11}\psi\nabla\frac{\delta F}{\delta\psi} + M_{12}\varphi\nabla\frac{\delta F}{\delta\varphi} \quad (26)$$

$$\mathbf{V}_c - \mathbf{V}^* = M_{21}\psi\nabla\frac{\delta F}{\delta\psi} + M_{22}\varphi\nabla\frac{\delta F}{\delta\varphi} \quad (27)$$

Substituting (26) into (15), we have

$$\frac{\partial\psi}{\partial t} + \nabla\cdot(\mathbf{V}^*\psi) = \nabla\cdot\left[L_{11}\nabla\frac{\delta F}{\delta\psi} + L_{21}\nabla\frac{\delta F}{\delta\varphi}\right] \quad (28)$$

Similarly, the equation for φ is given by

$$\frac{\partial\varphi}{\partial t} + \nabla\cdot(\mathbf{V}^*\varphi) = \nabla\cdot\left[L_{21}\nabla\frac{\delta F}{\delta\psi} + L_{22}\nabla\frac{\delta F}{\delta\varphi}\right] + \left[(2C*\Gamma_1)\frac{(1+\psi-\varphi)}{2}\frac{(1-\psi-\varphi)}{2} - \Gamma_{-1}\varphi\right] \quad (29)$$

In eqs 28 and 29, we have introduced $L_{11} = -\psi^2 M_{11}$, $L_{12} = L_{21} = -\psi\varphi M_{12}$, and $L_{22} = -\varphi^2 M_{22}$. M_{ij} are identical to those in Ohta's paper.[14] The Onsager coefficients L_{ij} depend on ψ,φ. However, because the explicit dependence on the friction coefficients ξ_i contained in M_{ij} is not specified within the present theory, we hereafter assume L_{ij} to be constants. We finally arrive at the following model equations:

$$\frac{\partial\mathbf{V}^*}{\partial t} + (\mathbf{V}^*\cdot\nabla)\mathbf{V}^* = \eta\nabla^2\mathbf{V}^* - \nabla p - \psi\nabla\frac{\delta F}{\delta\psi} - \varphi\nabla\frac{\delta F}{\delta\varphi} \quad (30)$$

$$\frac{\partial\psi}{\partial t} + \nabla\cdot(\mathbf{V}^*\psi) = L_{11}\nabla^2\frac{\delta F}{\delta\psi} + L_{21}\nabla^2\frac{\delta F}{\delta\varphi} \quad (31)$$

$$\frac{\partial\varphi}{\partial t} + \nabla\cdot(\mathbf{V}^*\varphi) = L_{21}\nabla^2\frac{\delta F}{\delta\psi} + L_{22}\nabla^2\frac{\delta F}{\delta\varphi} + \left[(2C^*\Gamma_1)\frac{(1+\psi-\varphi)}{2}\frac{(1-\psi-\varphi)}{2} - \Gamma_{-1}\varphi\right] \quad (32)$$

In line with the model equations adopted in the study of microemulsion, we employ the following TDGL equations:

$$\frac{\partial\mathbf{V}}{\partial t} + (\mathbf{V}\cdot\nabla)\mathbf{V} = \eta\nabla^2\mathbf{V} - \nabla p - \psi\nabla\frac{\delta F}{\delta\psi} - \varphi\nabla\frac{\delta F}{\delta\varphi} + \eta_\xi \quad (33)$$

$$\frac{\partial\psi}{\partial t} + \nabla\cdot(\mathbf{V}\psi) = M_\psi\nabla^2\frac{\delta F}{\delta\psi} + \eta_\psi \quad (34)$$

$$\frac{\partial\varphi}{\partial t} + \nabla\cdot(\mathbf{V}\varphi) = M_\varphi\nabla^2\frac{\delta F}{\delta\varphi} + \left[(2\Gamma_1)\frac{(1+\psi-\varphi)}{2}\frac{(1-\psi-\varphi)}{2} - \Gamma_{-1}\varphi\right] + \eta_\varphi \quad (35)$$

In the above TDGL equations, we have neglected the cross-coupling between ψ and φ fields, and we also assume $C^* = 1$. η_ψ, η_φ, and η_ξ represent the thermal noise which satisfies the fluctuation−dissipation theorem.

The free energy functional is assumed to be of the following form:[11]

$$F = \int \mathrm{d}r\,[w(\nabla^2\psi)^2 + d(\nabla\psi)^2 - a\psi^2 + u\psi^4 + e\varphi^2(\varphi-1)^2 - s\varphi(\nabla\psi)^2] \quad (36)$$

where the nonlocal coupling term $-s\varphi(\nabla\psi)^2$ favors species C sitting along A−B interfaces, reducing the surface tension, and the term $w(\nabla^2\psi)^2$prevents the model from being unbounded. In the discretization, $-a\psi^2 + u\psi^4$ is replaced by $-A\tanh\psi + \psi$ for the sake of numerical stability.

In the simulation, the parameters are set to 256 × 256 (size) with periodic boundary condition, $A = 1.3$, $w = 0.2$, $d = 0.5$, $s = 0.5$, $e = 0.25$, and $M_\psi = M_\varphi = 0.05$, which are the same as those in ref 11. The thermal noises are chosen as[11]

$$\eta_i = C_i[\eta_x(n_x+1,n_y,t) - \eta_x(n_x,n_y,t) + \eta_y(n_x,n_y+1,t) - \eta_y(n_x,n_y,t)] \quad (37)$$

where η_x,η_y are random numbers uniformly distributed in the interval $[-1,1]$, and C_i is the noise amplitude taken as $C_\psi = C_\varphi = C_\xi = 0.02$.

The above TDGL equations are solved by employing the cell dynamic scheme (CDS) proposed by Oono and Puri.[15] The discretization for the TDGL equations is similar to those used in the study of microemulsion.[9−12] The above model equations are similar to those employed in the study of microemulsion,[9−12] except the appearance of the chemical reaction term in (35). The above TDGL equations without the reaction term are double-checked both with and without hydrodynamic effect.

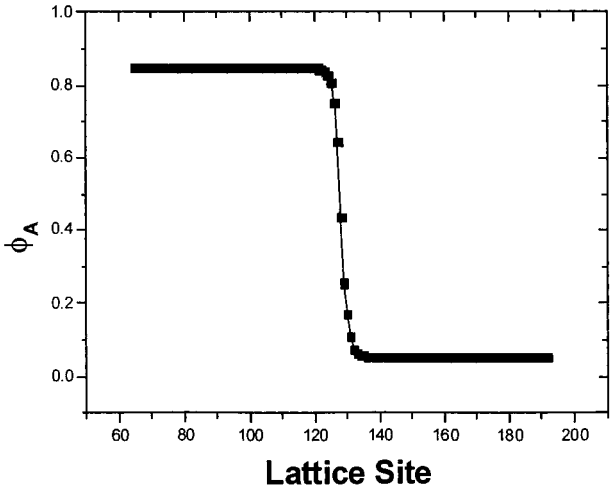

Figure 4. Concentration profile of species A along the direction perpendicular to the interface at steady state for the case of reaction rate constant $\Gamma_1 = \Gamma_{-1} = 0.01$.

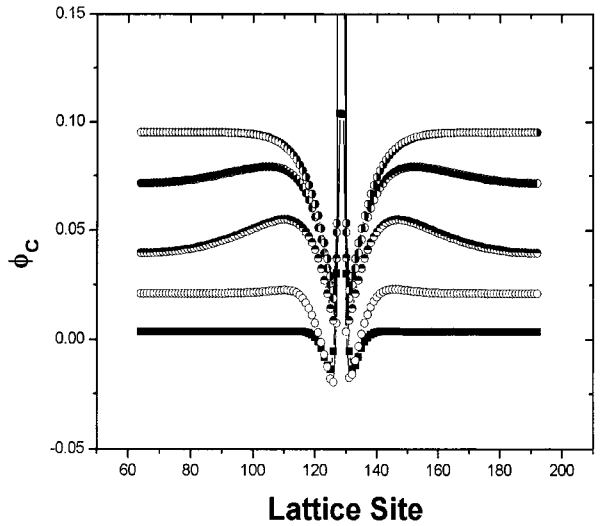

Figure 5. Time evolution profile from bottom to top of species C along the direction perpendicular to the interface for the case of reaction rate constant $\Gamma_1 = \Gamma_{-1} = 0.0001$.

Linearization of eqs 34 and 35 neglecting hydrodynamic effects at $\psi = 0$, $\varphi = 0$ state in Fourier space results in the following first-order differential equations for the fluctuations, $\delta\psi_k$, $\delta\varphi_k$, in the order parameters:

$$\frac{\partial}{\partial t}\delta\psi_k(t) = -k^2 M_\psi[-2a + 2k^4 w + 2k^2 d]\delta\psi_k(t) \quad (38)$$

$$\frac{\partial}{\partial t}\delta\varphi_k(t) = -[2eM_\varphi k^2 + \Gamma_1 + \Gamma_{-1}]\delta\varphi_k(t) \quad (39)$$

Therefore, the fluctuations can be expressed as

$$\delta\psi_k(t) = \delta\psi_k(0)\exp[-\gamma_1(k)t] \quad (40)$$

$$\delta\varphi_k(t) = \delta\varphi_k(0)\exp[-\gamma_2(k,\Gamma_{-1},\Gamma_1)t] \quad (41)$$

with

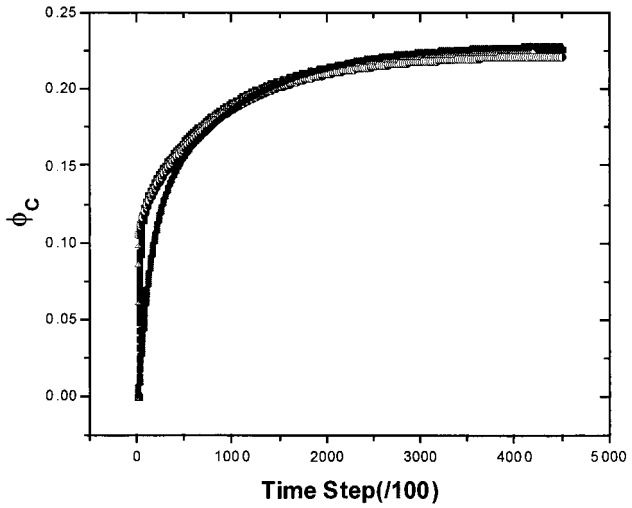

Figure 6. Time evolution profile of the averaged concentration of species C at different reaction rate constants (0.1, 0.01, 0.001, 0.0001, and 0.00001).

$$\gamma_1(k) = 2M_\psi[w\cdot k^6 + d\cdot k^4 - a\cdot k^2] \quad (42)$$

$$\gamma_2(k,\Gamma_{-1},\Gamma_1) = 2e\cdot M_\varphi\cdot k^2 + \Gamma_{-1} + \Gamma_1 \quad (43)$$

The most unstable mode $k = k_0$ which minimizes $\gamma_1(k)$ is

$$k_0 = \frac{-d + \sqrt{d^2 + 3aw}}{3w} \quad (44)$$

Then the typical time scale τ_0 in our model is given by

$$\tau_0 = \{1\}/\{[-\gamma_1(k_0)]\} \quad (45)$$

which is about 500 time steps.[11]

However, with regard to the chemical reaction rate constants, the linear stability analysis does not reveal any information concerning the existence of a cutoff wavelength at specific magnitude of rate constant.

III. Results and Discussion

A. Fixed Domain Size without Hydrodynamic Effect. Species A and B are put into each half of the box of size 256 × 256, respectively. To ensure numerical stability, a small amount of A or B is placed into B-rich or A-rich domain, respectively. The volume fraction is set at 0.96 for the rich phase and 0.04 for the other phase with fluctuation. The domains are equilibrated for 1000 time steps, and the interface profile is shown in Figure 1. Then the reaction is initiated. Parameter A is set to 1.2 to ensure numerical stability. The hydrodynamic effected is neglected.

1. Reversible $A + B \underset{\Gamma_{-1}}{\overset{\Gamma_1}{\rightleftharpoons}} C$. For simplicity, we assume $\Gamma_1 = \Gamma_{-1}$ and systematically vary the magnitude of rate constants (0.0001, 0.001, 0.01, 0.1). After the initiation of the chemical reaction, species C is generated along the interface as well as inside the A-rich or B-rich domains. The time evolution profile of average concentration of species C at different reaction rate constants is shown in Figure 2. It can be seen that the profiles nearly overlap with each other except that the evolution for $\Gamma = 0.0001$ is slower at the initial stage, and the steady-state concentration of C is almost the same regardless of the magnitude of the rate constants. The interface is a straight line without any corrugation. A prominent difference in cases of high and low reaction rate constants is the different magnitude of the concentration of species C along the interface at steady state as shown in Figure 3. Please note that, because of the periodic boundary condition, the interface is located at the top, middle, and the bottom of the 256 × 256 box. At higher rate constants ($\Gamma = 0.1$ and 0.01), the concentration of species C along the interface is only around 0.3. Whereas at lower rate

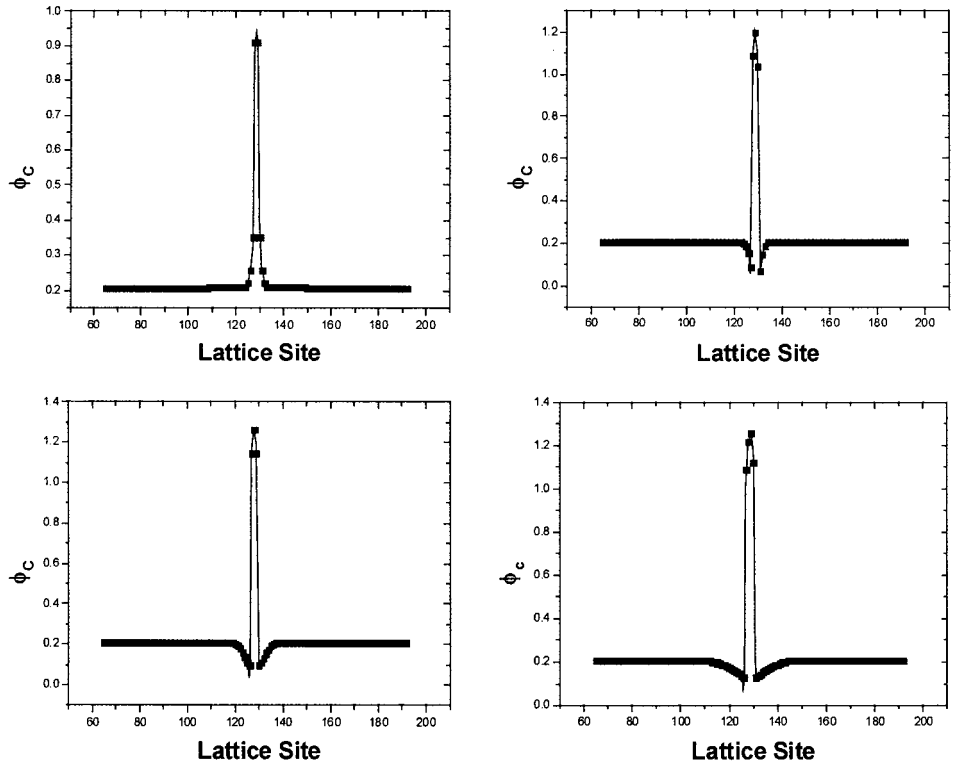

Figure 7. Steady-state concentration profile of species C along the direction perpendicular to the interface at different reaction rate constants. Top row: 0.1 for left, 0.01 for right. Bottom row: 0.001 for left, 0.0001 for right.

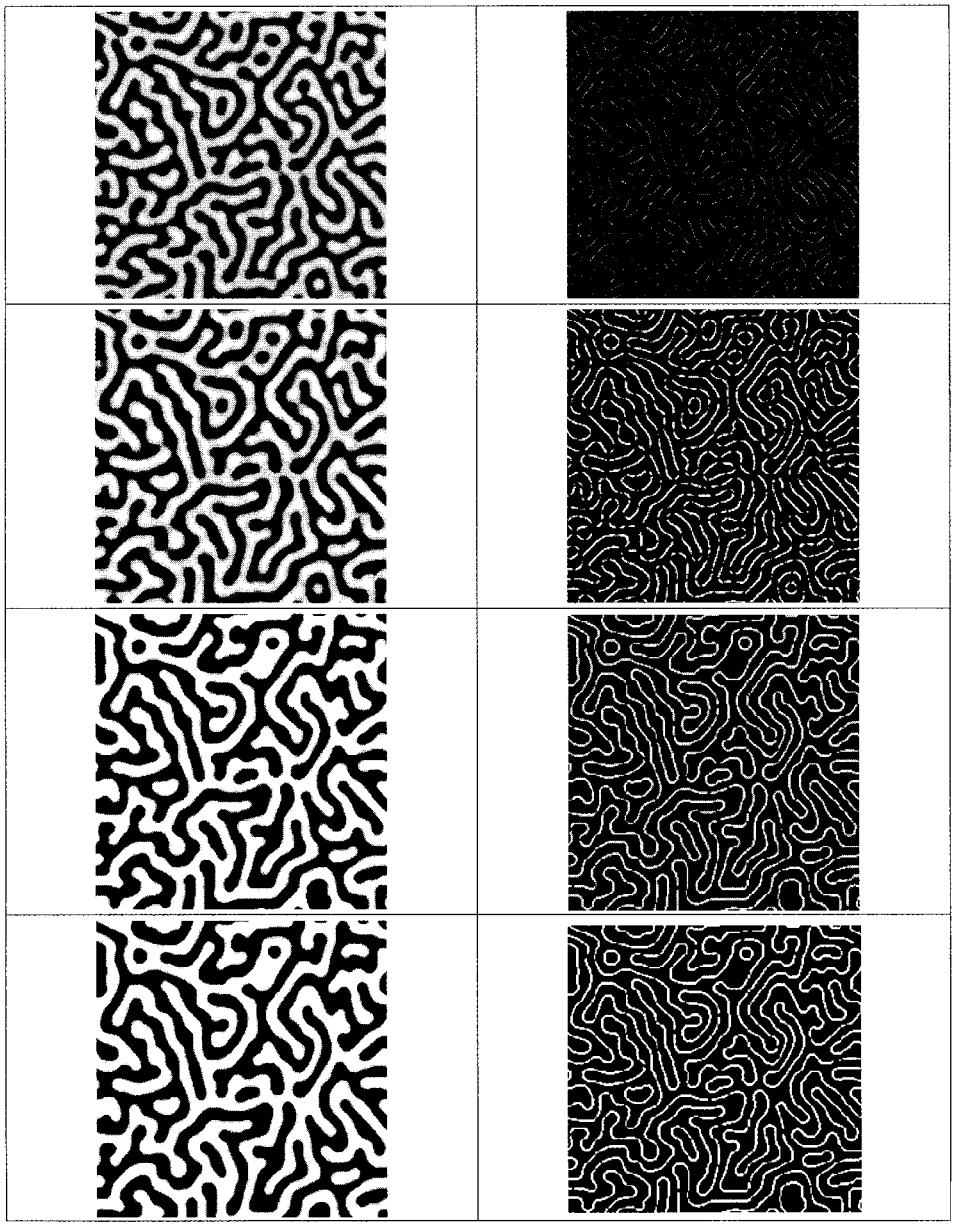

Figure 8. Evolution of domain patterns of reversible A + B ⇌ C at rate constant $\Gamma = 0.0001$ (time steps: 10.5k, 15k, 200k, and 2.4m from top to bottom). Left and right columns display the profile of order parameter ($\varphi_A - \varphi_B$) and concentration φ_C of species C, respectively.

constants ($\Gamma = 0.001$ and 0.0001), species C is saturated along the interface. Another notable feature of the reversible reaction is that in domains away from the interface the concentrations of species A, B, and C are very much close to chemical equilibrium for homogeneous reversible reaction. Figure 4 displays a typical concentration profile of species A along the direction perpendicular to the interface. From Figures 3 and 4, it can be seen that inside A-rich or B-rich domains, the concentration of C is around 0.1, whereas those of A or B are around 0.84 and 0.06, respectively; thus, $2\phi_A\phi_B \approx \phi_C$, satisfying eq 35 in homogeneous state. During the evolution of the chemical reaction and phase separation, species C generated along the interface gradually diffuses deeply into the domains rich in A and B until reaching the steady-state value of about 0.1. Figure 5 displays the time evolution profile of species C along the direction perpendicular to the interface at different time steps (1.5k, 5k, 20k, 100k, and 480k from bottom to top) for the case of reaction rate constant $\Gamma_1 = \Gamma_{-1} = 0.0001$. Similar behaviors are observed for cases of higher magnitude of rate constants.

2. Irreversible $A + B \xrightarrow{\Gamma_1} C$. We also investigated the phase separation dynamics and reaction kinetics for irreversible chemical reaction $A + B \xrightarrow{\Gamma_1} C$. Figure 6 dispalys the time evolution profile of the averaged concentration of species C at different reaction rate constants. It can be seen that, similar to the cases of the reversible reaction, the profiles nearly overlap with each other except that the evolution for $\Gamma = 0.0001$ is slower at the initial stage, and the steady-state concentration of C is almost the same regardless of the magnitude of the rate constants. For the irreversible reaction, the steady-state concentration is higher than that for the reversible reaction. In contrast to the case of the reversible reaction, the magnitude of the concentration of species C along the interface at steady state does not vary much for different rate constants as shown in Figure 7. Similar to the case of the reversible reaction, during the evolution of chemical reaction and phase separation, species C generated along the interface gradually diffuses deeply into the domains rich in A and B until reaching the steady state value of about 0.2. A notable difference between reversible and

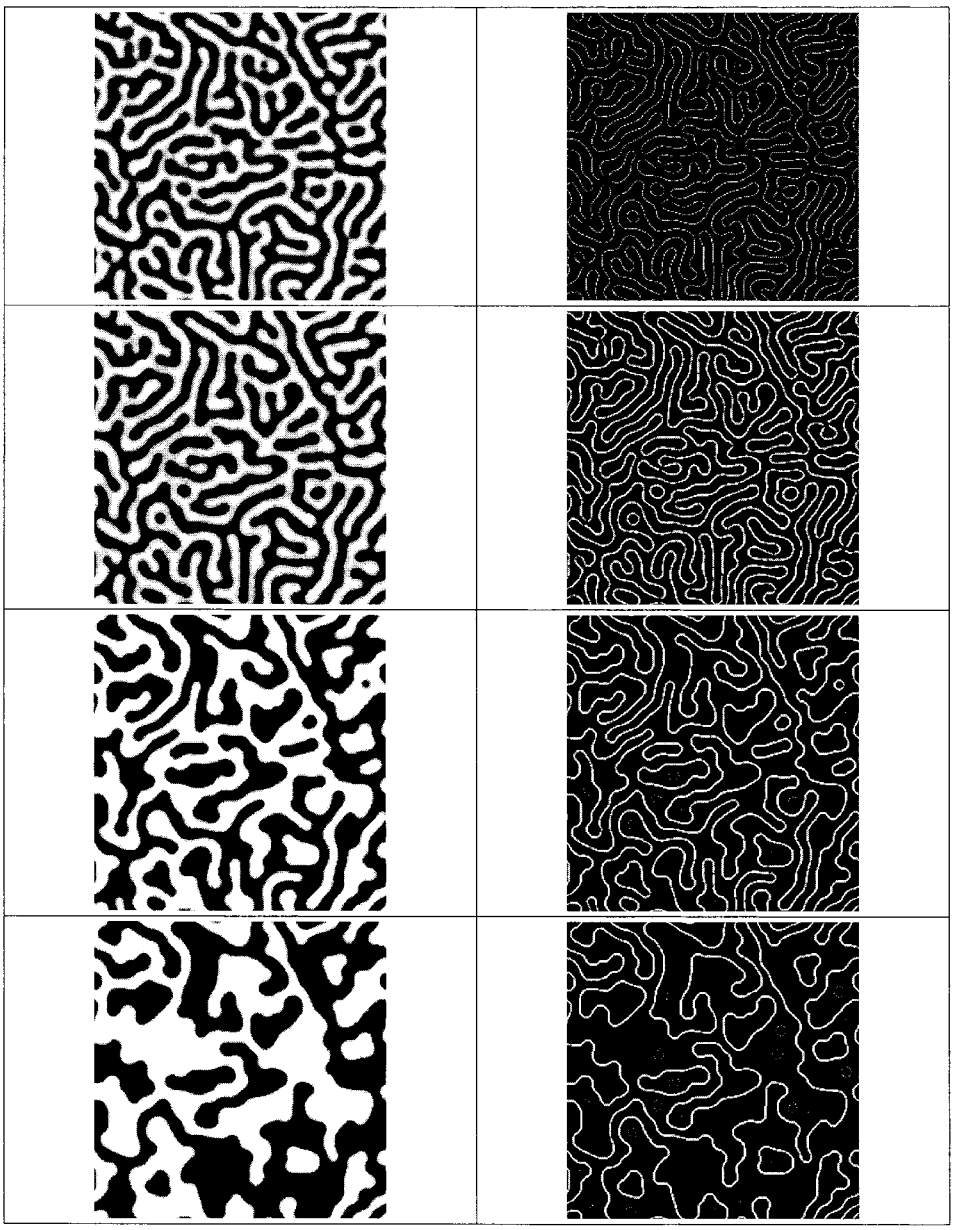

Figure 9. Evolution of domain patterns of reversible A + B ⇌ C at rate constant $\Gamma = 0.001$ (time steps: 10.5k, 15k, 200k, and 2.4m from top to bottom). Left and right columns display the profile of order parameter ($\varphi_A - \varphi_B$) and concentration φ_C of species C, respectively.

irreversible reactions is, for irreversible reaction, species A or B is completely depleted from the B-rich or A-rich phase, respectively, at steady state. It should be mentioned that the concentration profiles of species C shown in Figures 3, 5, and 7 are very steep along the interface. In our simulation, cell dynamic scheme (CDS) is employed to discretize the TDGL equations. In CDS, the lattice space of $x = 1$ is included implicitly. We have performed the discretization of TDGL equations in one dimension at position of index n and time step of index k, using

$$\frac{\partial \phi}{\partial x}\Big|_n^k = \frac{\phi_{n+1}^k - \phi_{n-1}^k}{2x} \tag{46}$$

$$\frac{\partial^2 \phi}{\partial x^2}\Big|_n^k = \frac{\phi_{n+1}^k - 2\phi_n^k + \phi_{n-1}^k}{\Delta x^2} \tag{47}$$

$$\frac{\partial \phi}{\partial t}\Big|_n^k = \frac{\phi_n^{k+1} - \phi_n^k}{\Delta t} \tag{48}$$

Because of the highest derivative in our TDGL equations is 6th, the numerical stability requirement is $\{\nu\Delta t\}/\{\Delta.x^6\}$, smaller than 1/2, where ν is the numerical coefficient in front of the 6th term. We vary Δx from 1 to 0.5, 0.25, and 0.125, and accordingly, reduce Δt 64 times successively. The steep profiles of species C still persist even with the reduction of mesh size. We think that the steep profiles of C are due to the term $\varphi^2(1 - \varphi)^2$ in the free energy functional. For reversible reaction, at high reaction rate constants, the effect of the chemical reaction is strong, the species C at the interface approximately satisfies the chemical reaction equilibrium relation $2\phi_A\phi_B \approx \phi_C$, and the profile is relatively smooth. However, when the reaction rate constants are relatively small, the effect of phase separation is dominant, the $\varphi^2(1 - \varphi)^2$ term strongly favors the saturation of species C at the interface; therefore, the concentration profile of C is steep. For the irreversible reaction, C formed at the interface saturates because of the $\varphi^2(1 - \varphi)^2$ term, so the profiles of C are steep regardless of the magnitude of the reaction rate constants.

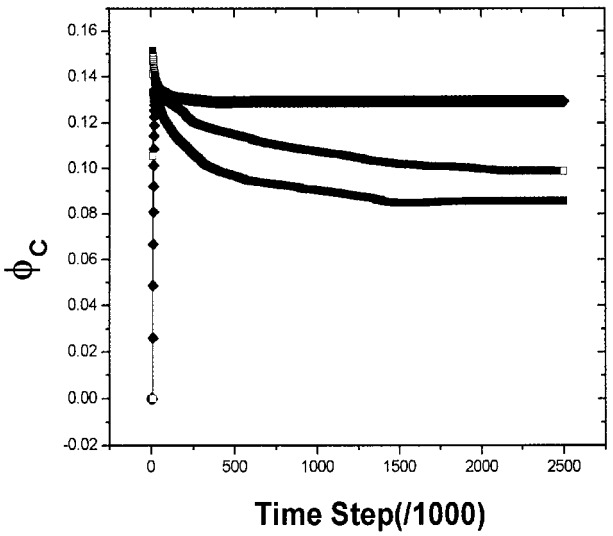

Figure 10. Evolution profiles of the averaged concentration of species C for reversible reaction at rate constants $\Gamma = 0.0001$, 0.0003 and 0.001 from top to bottom.

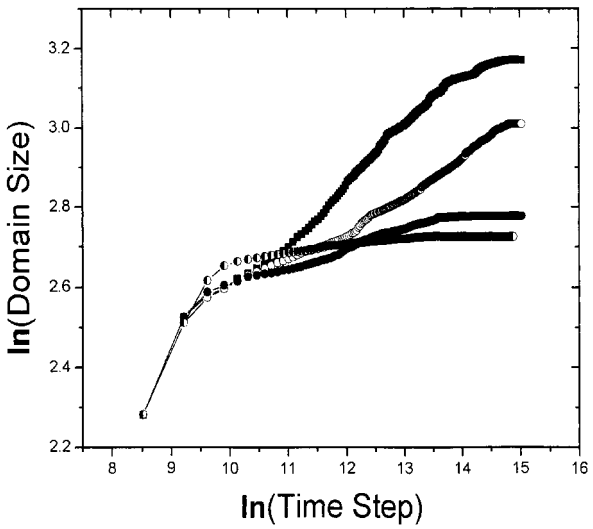

Figure 11. Double logarithm evolution profiles of domain size of the A-rich or B-rich phases for the reversible reaction at rate constants $\Gamma = 0.0001$, 0.0006, 0.0003, and 0.001.

B. Coupling of Domain Growth and Chemical Reaction without Hydrodynamic Effect. A binary mixture of A and B is quenched to a lower temperature and phase separates. After 10 thousand time steps, chemical reaction is turned on. Because of numerical instability at $\Gamma > 0.001$ which cannot be resolved either by reducing the quenching depth or shortening the time steps, we only concentrate on the phase separation dynamics and reaction kinetics at smaller reaction rate constants $\Gamma = 0.001$, 0.0006, and 0.0003, 0.0001. The evolution of domain patterns of reversible A + B $\rightleftharpoons$ C at rate constant $\Gamma = 0.0001$ and 0.001 are shown in Figures 8 and 9, respectively. It can be seen from Figure 8 that 500 time steps after the initiation of the reaction, there is a little amount of species C emerging along the interface between A-rich and B-rich domains. As shown in Figure 10, the concentration of species C at $\Gamma = 0.0001$ gradually increases up to a maximum value at about 30000 time steps, it then begins to decrease and gradually reaches steady-state value (top profile). Whereas for higher rate constants of $\Gamma = 0.001$ and 0.003, species C quickly reaches a maximum value and then slowly decomposes along the interface and also gradually reaches the steady-state value, which is smaller for higher reaction rate constants. The evolution profiles of domain sizes at $\Gamma = 0.001$, 0.0006, and 0.0003 as well as 0.0001 are shown in Figure 11. The domain sizes which are averaged over three different initial conditions are calculated using the "broken bonds" formula proposed by Ohta,[16] in which the characteristic size is the inverse "area" density, $R = \{L^d\}/\{A(t)\}$, where L^d is the "volume" of the system and $A(t)$ is the total "area" of the interface. For a two-dimensional system, the formula reads $R = \{L^2\}/\{(N_x + N_y)\}$, where N_x and N_y are the numbers of "broken bonds" (pairs of nearest neighboring sites with opposite signs of order parameter $\phi_A - \phi_B$) in the x and y directions, respectively. This evaluation of characteristic length scale is found not to differ from the method used in microemulsion.[11] From Figure 11, it can be seen that the domain growth eventually freezes for all cases of reaction rate constants. The higher the reaction rate constants are, the slower the evolution to reach steady state is and the larger the steady state domain size is. Phase separation dynamics of the oil−water/surfactant system has been studied, and it is shown that the surfactant segregates along the oil−water interface lowering the interfacial tension, and the domain growth eventually freezes because of the decrease of the driving force of domain growth. In our present study, domain growth eventually freezes and reversible chemical reaction and phase separation reach steady state.

We would also like to see the hydrodynamic effect on phase separation coupled with interfacial interaction. Unfortunately, the hydrodynamic effect causes numerical instability at $\Gamma > 0.0001$ and prevents us from investigating the hydrodynamic effects at relatively higher reaction rate constants.

IV. Conclusion

In this paper, we investigated the reaction kinetics and phase separation dynamics of a ternary mixture of A, B, and C coupled with an interfacial chemical reaction A + B $\rightleftharpoons$ C, taking into account of the effect of reduction of interfacial tension of species C. We studied the system with domain size fixed and normal domain growth system. In the case of fixed domain size, the chemical equilibrium of the reactive species is observed inside either an A-rich or B-rich domain (half box) for the reversible reaction. Whereas for the irreversible reaction, A (or B) is depleted in B (or A)-rich domain. Also, for the case of fixed domain size, it was found that the change of reaction rate constants does not exert appreciable influence on the concentration profile of reacting species and the process is diffusion-controlled, consistent with the theoretical studies by Fredrickson and Milner.[17] However, recent experimental studies by Dr. Macosko's group[18] suggest that the block copolymer formation along the polymer interface is limited by reaction rate. We think these are the two different aspects of the interfacial reaction of the phase-separating system. In their experiments, the samples were annealed at a high temperature (174 °C), where the diffusion of the polymer chains is very fast. In this paper, we only focused on the diffusion-limited process.

In the cases of coupling between domain growth and reversible reaction kinetics, it was shown in simulations that the domain growth eventually freezes in all cases of low and high reaction rate constants. The higher the reaction rate constants are, the slower the evolution to reach the reach steady state is, the larger the steady state domain size is, and the smaller the average concentration of species C is. A phenomenological explanation is that, at a higher reaction rate constant, the decomposition of species C at the interface because of the backward reaction accelerates; therefore, less of an amount of C is segregated along the interface, which allows larger domain

growth at the steady state. In our simulation, species C permanently stays along the interface after reaching steady state concentration. In our previous study in which the effect of reduction of interfacial free energy due to existence of species C along the interface is neglected, species C decomposes exponentially along the interface and is quickly consumed, and the exponent is proportional to the magnitude of reaction rate constants. In contrast to our previous study, here we observed that species C along the interface is much more stable, because of the reduction of the interfacial free energy of species C along the interface. As the first attempt to simulate the interfacial reaction coupled with phase separation, a mimic of reactive blending, we in our model did not take into account the polymer architecture, which has the restriction that only end-functionalized polymer chains of different kinds can react when they meet with each other. Inclusion of polymer architecture could be done using the dynamical mean field method shown by Yeung and Shi.[19] We are currently studying the interfacial reaction coupled with phase separation with polymer architecture included using a dynamical mean field.

Acknowledgment. This work was supported by the Special Funds for Major State Basic Research Projects (G1999064800). We would also like to thank Professor Z. -G. Wang from CALTECH, Pasadena, CA for valuable suggestions.

References and Notes

(1) Gompper, G.; Schick, M. *Self-Assembling Amphiphilic Systems*, Academic Press: London, 1994.
(2) Lyatskaya, Y.; Gersappe, D.; Gross, N. A.; Balazs, A. C. *J. Phys. Chem.* **1996**, *100*, 1449.
(3) O'Shaughnessy, B.; Sawhney, U. *Macromolecules* **1996**, *29*, 7230.
(4) O'Shaughnessy, B.; Vavylonis, D. *Macromolecules* **1999**, *32*, 1785.
(5) O'Shaughnessy, B.; Vavylonis, D. *Eur. Phys. J. B* **1998**, *6*, 363.
(6) Bychuk, O. V.; O'Shaughnessy, B.; Turro, N. J. *Eur. Phys. J. E* **2001**, *4*, 281.
(7) Liu, B.; Tong, C.; Yang, Y. *J. Phys. Chem. B* **2001**, *105*, 10091.
(8) Tong, C.; Yang, Y. *J. Chem. Phys.* **2002**, *116*, 1519.
(9) Roan, J.-R.; Shakhnovich, E. I. *Phys. Rev. E* **1999**, *59*, 2109.
(10) Roan, J.-R.; Hu, C.-K. *Phys. Rev. E* **2000**, *62*, 766.
(11) Komura, S.; Kodama, H. *Phys. Rev. E* **1997**, *55*, 1722.
(12) Patzold, G.; Dawson, K. *Phys. Rev. E* **1995**, *52*, 6908.
(13) Doi, M. *Springer Proc. Phys.* **1990**, *52*, 100.
(14) Nonomura, M.; Ohta, T. *J. Chem. Phys.* **1999**, *110*, 7516.
(15) Oono, Y.; Puri, S. *Phys. Rev. Lett.* **1987**, *58*, 836; *Phys. Rev. A* **1988**, *38*, 434.
(16) Ohta, T.; Jasnow, D.; Kawasaki, K. *Phys. Rev. Lett.* **1982**, *49*, 1223
(17) Fredrickson, G. H.; Milner, S. T. *Macromolecules* **1996**, *29*, 7386.
(18) Schulze, J. S.; Cernohous, J. J.; Hirao, A.; Lodge, T. P.; Macosko, C. W. *Macromolecules* **2000**, *33*, 1191.
(19) Yeung, C.; Shi, A. C. *Maromolecules* **1999**, *32*, 3637.